# Motility-Induced Temperature Difference in Coexisting Phases

Suvendu Mandal,[1,*] Benno Liebchen,[1,2,†] and Hartmut Löwen[1,‡]
[1]Institut für Theoretische Physik II: Weiche Materie, Heinrich-Heine-Universität Düsseldorf, D-40225 Düsseldorf, Germany
[2]Theorie Weicher Materie, Fachbereich Physik, Technische Universität Darmstadt, Hochschulstraße 12, 64289 Darmstadt, Germany

(Received 21 May 2019; published 26 November 2019)

Unlike in thermodynamic equilibrium where coexisting phases always have the same temperature, here we show that systems comprising "active" self-propelled particles can self-organize into two coexisting phases at different kinetic temperatures, which are separated from each other by a sharp and persistent temperature gradient. Contrasting previous studies that have focused on overdamped descriptions of active particles, we show that a "hot-cold coexistence" occurs if and only if accounting for inertia, which is significant, e.g., in activated dusty plasmas, microflyers, whirling fruits, or beetles at interfaces. Our results exemplify a route to use active particles to create a self-sustained temperature gradient across coexisting phases. This phenomenon is fundamentally beyond equilibrium physics and is accompanied by a slow coarsening law with an exponent significantly smaller than the universal $1/3$ exponent seen in both equilibrium systems and overdamped active Brownian particles.

DOI: 10.1103/PhysRevLett.123.228001

*Introduction.*—In equilibrium systems, entropy maximization (or free energy minimization) requires thermal, mechanical, and chemical equilibrium among coexisting phases. Conversely, in nonequilibrium no fundamental law forbids different temperatures in coexisting phases, evoking the question if a specific mechanism exists that can generate such a difference. Such a mechanism may appear counterintuitive, as heat gradients, unless they are sustained by a localized heat source such as a star performing nuclear fusion, usually cause processes opposing them and driving the system towards thermal equilibrium (unless for ideal isolation): For example, a temperature difference in the air evokes a balancing wind, and air friction cools down a radiator once switched off.

Here we report and systematically explore a surprisingly different scenario, where particles self-organize into coexisting phases sustaining different temperatures. This two temperature coexistence occurs spontaneously in a uniform system and, remarkably, there is no heat flux at steady state, because the gradient in kinetic temperature is balanced by a self-sustained, opposite density gradient. A "hot" and a "cold" phase are allowed to coexist in principle, as the system we consider comprises self-propelled microparticles which allow the system to bypass equilibrium thermodynamics.

By now, we know that such microparticles, often described as "active Brownian particles" [1–5], can self-organize into a liquid phase, coexisting with a gas phase, even when interacting purely repulsively [6–17]. Coined as "motility-induced phase separation," or MIPS, this phenomenon has advanced to a key paradigm in the physics of self-propelled particles. When the microparticles are overdamped, like microorganisms in a solvent [18] or active colloidal microswimmers [19–23], they are equally fast in both phases. Hence, despite the presence of active microparticles, liquid and gas as emerging from MIPS have identical kinetic temperatures, just like for liquid-gas phase separation in equilibrium. (Note that MIPS involves a slow down of particles in regions of high density [2,6], which occurs, however, only for the "coarse grained self-propulsion," not for the actual velocity determining the kinetic temperature, as further discussed below.)

When releasing the overdamped standard approximation, as relevant, e.g., for beetles at interfaces [24], whirling fruits [25], microflyers [26] or activated dusty plasmas [27], both the phase diagram and the properties of the contained phases change dramatically, as we show in this Letter. In particular, while MIPS generally requires a sufficiently large self-propulsion speed $v_0$ to occur, specifically for underdamped particles, it breaks down again if $v_0$ is too large; i.e., MIPS is reentrant in the presence of inertia [28]. This is because MIPS also requires particles to slow down (regarding their directed motion) in regions of high density [2]: such a slow down occurs instantaneously upon collisions of overdamped particles, but in the presence of inertia, particles bounce back from collisions and do not slow down much before experiencing subsequent collisions. Thus, at very large $v_0$, underdamped particles can exchange their kinetic energies before slowing down much and MIPS breaks down.

To see which physical mechanism controls the difference in kinetic temperature (which is identical to the virial temperature and to be distinguished from the effective temperature [29–32]) in coexisting phases, consider the collision of an active underdamped particle moving with a fixed orientation towards an elastically reflecting wall.

 

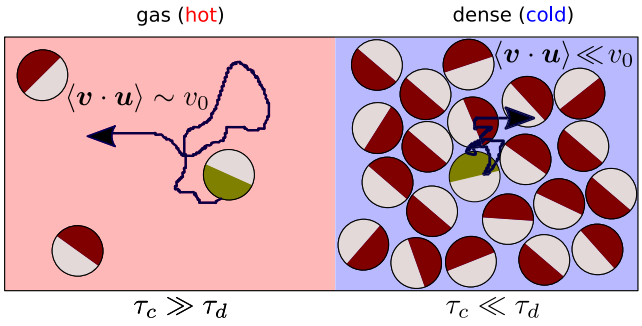


FIG. 1. Scheme of the phase-separated state associated with a hot-cold coexistence in underdamped active particles. Particles self-propel with the colored cap ahead (brown; greenish for the tagged particle). Active particles move with $\sim v_0$ in the gas phase, but can be an order of magnitude slower in the dense phase.

This problem is equivalent to a bouncing ball experiencing friction and gravity (see Supplemental Material [33] for details): while reaching a terminal speed ($v_0$) when falling in free space, the ball continuously slows down, when reflected by a wall, even when the collisions are elastic. Analogously, particles essentially move with $v_0$ in the gas phase, where they rarely collide, but slow down when entering the dense liquid phase, due to successive collisions with other particles (see Fig. 1). Notice that inelastic collisions among the particles provide an alternative, but mechanistically unrelated, route to achieve a remarkable hot-cold coexistence, which has been discussed for vibrated granular particles, where particles dissipate energy due to inelastic collisions [39–41]. In contrast, for the microparticles we consider, no inelastic collisions are required: the emergence of coexisting temperatures is based on the interplay of activity and weak inertia.

Our results exemplify a generic route to use active particles to create a self-sustained temperature gradient across coexisting phases, a phenomenon which is fundamentally beyond equilibrium physics. This contrasts the overdamped standard case, which has been predominantly explored in active matter physics so far and leads to the dynamics which are diffusive and curvature driven and therefore can be essentially mapped onto an equilibrium system at a coarse-grained level [2,6] yielding a phase transition that is consistent with an equilibrium liquid-gas transition [16]. Thus, the existence of temperature differences in coexisting phases indicates a change of the nature of MIPS, when releasing the overdamped standard approximation, resulting in a significant deviation from the universal $t^{1/3}$ coarsening law for the mean cluster size, as we will show. Accordingly, MIPS [6,42–45], a key result in active matter physics, has remarkable consequences that are fundamentally beyond equilibrium physics even at a coarse-grained level, but have been curtained by the overdamped standard approximation in previous studies.

*Model.*—Let us now consider a generic model for active underdamped particles in two dimensions, each having an internal drive, represented by an effective self-propulsion force $\mathbf{F}_{\mathrm{SP},i} = \gamma_t v_0 \mathbf{u}(\theta_i)$, where $\mathbf{u}(\theta_i) = (\cos\theta_i, \sin\theta_i)$ is the direction of self-propulsion. The particles have identical diameters $\sigma$, masses $m$, and moments of inertia $I$. They interact via an excluded-volume repulsive force $\mathbf{F}_i$ (see Supplemental Material [33]). Their velocities $\mathbf{v}_i$ and orientations $\theta_i$ evolve as

$$m\frac{d\mathbf{v}_i}{dt} = -\gamma_t \mathbf{v}_i + \mathbf{F}_i + \mathbf{F}_{\mathrm{SP},i} + \sqrt{2k_B T_b \gamma_t}\boldsymbol{\eta}_i(t),$$
$$I\frac{d^2\theta_i}{dt^2} = -\gamma_r \frac{d\theta_i}{dt} + \sqrt{2k_B T_b \gamma_r}\xi_i(t), \quad (1)$$

where $\boldsymbol{\eta}_i$, $\xi_i$ represent Gaussian white noise of zero-mean unit variance, $T_b$ is the effective bath temperature, and $\gamma_t, \gamma_r$ are translational and rotational drag coefficients, yielding diffusion coefficients $D_{t,r} = k_B T_b/\gamma_{t,r}$. To understand the behavior of active underdamped particles, it is instructive to define three characteristic timescales (see Table I): the persistence time $\tau_p = 1/D_r$, after which the directed motion of active particles is randomized by rotational diffusion, the mean time between collisions for a given particle $\tau_c = \pi\sigma/(4v_0\varphi)$, where $\varphi = N\pi\sigma^2/(4L_x L_y)$ is the area fraction, and the inertial timescale $\tau_d = m/\gamma_t$, characterizing the time a particle at rest needs to reach its terminal speed. In principle, the moment of inertia $I$ leads to an additional timescale $(I/\gamma_r)$, but it turns out to be largely irrelevant to our results and is thus kept constant to $I = 0.33\epsilon\tau_p^2$, see Supplemental Material [33].

TABLE I. Relevant timescales in active underdamped particles.

| | |
|---|---|
| Persistence time | $\tau_p = 1/D_r$ |
| Mean time between collisions | $\tau_c = \pi\sigma/(4v_0\varphi)$ |
| Inertial time | $\tau_d = m/\gamma_t$ |

Fixing the area fraction to a regime where MIPS can occur ($\varphi = 0.5$), the behavior of our system is mainly controlled by two parameters, which can be expressed as ratios of the relevant timescales: $M = \tau_d/\tau_p$, which is a reduced mass measuring the impact of inertia, and the Péclet number $\mathrm{Pe} = v_0/(D_r\sigma) \propto \tau_p/(\tau_c\varphi)$, measuring the strength of self-propulsion by comparing ballistic to a diffusive motion.

*Nonequilibrium phase diagram.*—To explore the impact of inertia on the collective behavior of active particles, we first investigate the phase diagram using large-scale simulations based on LAMMPS [46]. If $M \to 0$, inertia plays no role and the particles are essentially overdamped. Accordingly, for $M \lesssim 10^{-4}$, we recover the usual behavior: at fixed area fraction $\varphi = 0.5$, the particles undergo MIPS [10,12] when the Péclet number is large enough ($\mathrm{Pe} \gtrsim 20$), leading to a dense liquid phase, coexisting with a gas phase [Fig. 2(a)]. For moderate inertia ($0.03 \leq M \leq 0.07$), we still require Pe to exceed a certain threshold to allow the

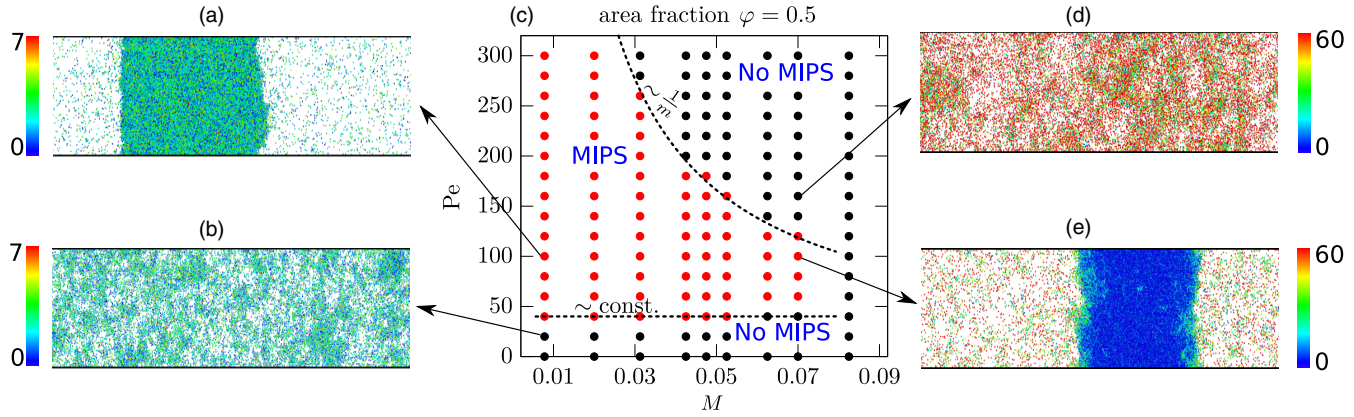


FIG. 2. Nonequilibrium phase diagram at $\varphi = 0.5$ (c). Panels (a), (b), (d), and (e) represent snapshots from our simulations ($L_x \times L_y = 350\sigma \times 70\sigma$) at state points indicated in the phase diagram. Colors represent kinetic energies of individual particles in units of $k_B T_b$. A hot-cold coexistence is visible in panel (e). Dashed lines in (c) show scaling predictions for the phase boundary between the homogeneous and phase-separated state.

system to phase separate into a liquid and a coexisting gas [Fig. 2(e)]. However, when further increasing Pe, strikingly, MIPS disappears and the system remains in the disordered phase [Fig. 2(d)]. Thus, MIPS is reentrant for underdamped active particles. Finally, when inertia is even stronger $M \gtrsim 0.08$, MIPS does not occur at all. Overall, this leads to the phase diagram shown in Fig. 2(c). The qualitative structure of this phase diagram can be understood based on simple scaling arguments. To see this, let us first remember how MIPS arises for overdamped particles: consider a particle self-propelling towards a small dense cluster of particles; when colliding, the particle stops and is blocked by the cluster, until rotational diffusion turns its self-propulsion direction away from the cluster on a timescale $\tau_p = 1/D_r$. When the time in between collisions $\tau_c$ is smaller than $\tau_p$, the rate of particles entering the cluster exceeds the leaving rate and the cluster rapidly grows [7,9], later proceeding slowly towards phase separation. This criterion explains the existence of a (lower) critical Péclet number. Since both $\tau_c$, $\tau_p$ are mass independent, we expect the lower critical Pe number also to be mass independent:

$$\tau_p \gtrsim \tau_c \Rightarrow \mathrm{Pe}_1 = \text{const}, \tag{2}$$

as approximately observed in Fig. 2(c). To understand the upper critical Pe number, note that MIPS requires a localized slow down of particles to occur. Thus, at very high collision rates (due to high Pe), underdamped particles bounce back multiple times on the inertial timescale $\tau_d$, and can therefore not slow down locally. We, therefore, expect that MIPS occurs only if

$$\tau_c \gtrsim \tau_d \Rightarrow \mathrm{Pe}_2 \propto 1/m, \tag{3}$$

which yields the scaling law $\mathrm{Pe}_2 \sim 1/m$ shown as the upper dashed line in Fig. 2(c) and corresponds to our simulation results.

*Temperature difference in coexisting phases.*—While in the overdamped case ($M \to 0$), particles in the liquid and in the coexisting gas are equally fast on average as shown by the colors in Fig. 2(a), this changes dramatically when inertia becomes significant. Following the colors in Fig. 2(e) we see, strikingly, that particles in the liquid (blue dots) are much slower than in the gas (green, yellow, and red dots). Before discussing the origin of this remarkable temperature difference, let us quantify it in more detail. To this end, we define the kinetic temperature as $T_{\mathrm{eff}}(x) = \frac{1}{2} m \langle v^2(x) \rangle$, which is the kinetic energy per particle, averaged along the lateral coordinate. Unlike various other approaches that can be used to define temperature in equilibrium, the kinetic temperature and the virial temperature are both well defined also for active systems and are identical to each other (see Supplemental Material [33]). As shown in Fig. 3(a), $T_{\mathrm{eff}}$ is uniform for $M = 10^{-5}$, but develops a massively nonuniform shape when increasing $M$ to 0.05 (see Supplemental Material [33], Movies S1 and S2, respectively). Figure 3(c) quantifies the resulting temperature difference, showing $(T_{\mathrm{gas}} - T_{\mathrm{dense}})/T_{\mathrm{dense}}$ as a function of $M$. Here, we see that the temperature in the dilute phase can be almost 2 orders of magnitude larger than in the dense phase. This is further reflected by the velocity distribution $P(v_x)$ in Fig. 3(b), showing a far-broader distribution for the gas phase than for the dense one, but only if inertia is significant (see inset). For the gas phase, a non-Gaussian tail appears at larger velocities [47].

*Power balance.*—To understand the temperature difference quantitatively, we now derive a power-balance equation. Multiplying the translational part of Eq. (1) by $\mathbf{v}$, and averaging over all particles in a given phase, we obtain

$$\frac{1}{2} m \frac{d\langle v^2(t) \rangle}{dt} = -\gamma_t \langle v^2(t) \rangle + \langle \mathbf{v}(t) \cdot \mathbf{F}(t) \rangle + \langle \mathbf{v}(t) \cdot \mathbf{F}_{\mathrm{SP}}(t) \rangle + \sqrt{2 k_B T_b \gamma_t} \langle \mathbf{v}(t) \cdot \boldsymbol{\eta}(t) \rangle. \tag{4}$$

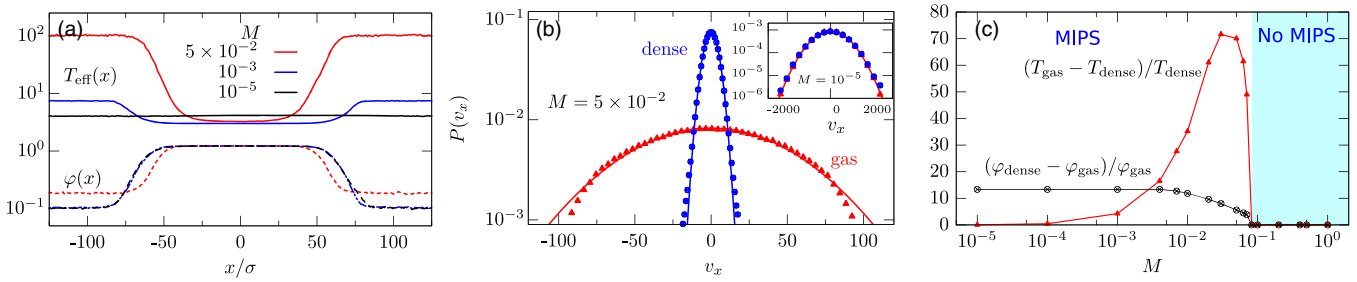


FIG. 3. (a) Spatial profiles of the effective temperature $T_{\rm eff}(x)+2.0$ (solid lines) and local area fraction $\varphi(x)$ (dashed lines) for different reduced masses $M$. (b) Steady-state distributions of particle velocities $v_x$ for moderate inertia $M=5\times10^{-2}$. Solid lines are fits to the Maxwell-Boltzmann distribution $P(v_x)=\sqrt{m/(2\pi T_{\rm eff})}\exp[-mv_x^2/(2T_{\rm eff})]$, where $T_{\rm eff}$ is the kinetic temperature. Inset: $P(v_x)$ for vanishing inertia $M=10^{-5}$. (c) The relative temperature and area fraction difference between the two phases as a function of inertia. Other parameters: Pe $=100$, $\varphi=0.5$.

Here, the left-hand side equals the time derivative of the effective temperature $\partial T_{\rm eff}/\partial t$; $\gamma_t\langle v^2(t)\rangle=2T_{\rm eff}/\tau_d$ describes the energy dissipation rate due to Stokes drag and $\langle\mathbf{v}(t)\cdot\mathbf{F}(t)\rangle$ represents the dissipated power due to interactions among the particles, which is negligible here since particle collisions are elastic, see Supplemental Material, Fig. S4 [33]. The third term $\langle\mathbf{v}(t)\cdot\mathbf{F}_{\rm SP}(t)\rangle$ represents the self-propulsion power. The last term is related to the bath temperature by the following relation $\sqrt{2k_BT_b\gamma_t}\langle\mathbf{v}(t)\cdot\boldsymbol{\eta}(t)\rangle=2k_BT_b\gamma_t/m=2k_BT_b/\tau_d$, which is identical in the gas and in the dense phase. Plugging these expressions into Eq. (4), and using that $\partial T_{\rm eff}/\partial t=0$ in each phase individually in steady state, we obtain

$$T_{\rm gas}-T_{\rm dense}=\frac{\tau_d}{2}[\langle\mathbf{v}\cdot\mathbf{F}_{\rm SP}\rangle_{\rm gas}-\langle\mathbf{v}\cdot\mathbf{F}_{\rm SP}\rangle_{\rm dense}]. \quad (5)$$

Therefore, if and only if $\tau_d\neq0$, self-propulsion can create a temperature difference in coexisting phases. Since $\tau_d=0$, in overdamped particles, both phases have the same kinetic temperature. In contrast, for underdamped particles we have $\tau_d\neq0$. The contributions of the individual terms to the power balance is visualized in Supplemental Fig. S4 [33], revealing that the self-propulsion power is much higher in the gas phase than in the dense phase and dominates the kinetic temperature (rather than diffusion as for overdamped particles). To see why the self-propulsion power is different in the gas phase compared to the dense phase, we explore the distribution of the particle effective speeds $v_{\rm eff}=\mathbf{v}\cdot\mathbf{u}$ in both phases; here $\langle\mathbf{v}\cdot\mathbf{F}_{\rm SP}\rangle=\gamma_t v_0\langle v_{\rm eff}\rangle$. Thus, Fig. 4(a) shows that the average effective speed in the gas phase is $v_0$, whereas negative speed values are rare, showing that particles in the gas phase rarely move against their self-propulsion direction (Fig. 1, left panel). This suggests that $\langle\mathbf{v}\cdot\mathbf{F}_{\rm SP}\rangle_{\rm gas}\sim\gamma_t v_0^2$. In contrast, in the dense phase, the effective particle speed is almost symmetrically distributed around 0, which results from the fact that particles have no space to move and bounce back after each collision; thus, they move against their self-propulsion direction about half of the time (Fig. 1, right panel), which implies $\langle\mathbf{v}\cdot\mathbf{F}_{\rm SP}\rangle_{\rm dense}\sim0$.

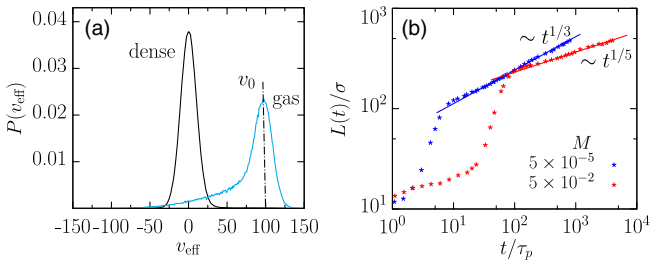


FIG. 4. (a) Probability distributions of effective speeds in the gas phase as well as in the dense phase for $M=10^{-2}$. (b) $L(t)$ for overdamped (blue symbols) and underdamped (red symbols) particles with power law fits (solid lines). Other parameters: Pe $=100$, $\varphi=0.5$.

Finally, to be more explicit about the essential difference regarding the nature of MIPS, respectively, for inertial and overdamped particles let us explore their characteristic coarsening behavior. Recall first that overdamped ABPs which can be mapped onto an equilibrium system at coarse-grained scales [6] and therefore lead to the same universal $L(t)\propto t^{1/3}$ coarsening law characterizing equilibrium systems [10,44], where $L(t)$ is the mean cluster size at late times, which we calculate from the first moment of the static structure factor $S(q,t)$ [10]. Conversely, underdamped active particles do not allow for such a mapping, because uniform temperature profiles are not possible in equilibrium. Our simulations reflect this fundamental difference between overdamped and underdamped active particles and indicate a coarsening law of $L(t)\propto t^{1/5}$ for the latter case [see Fig. 4(b) and Supplemental Material [33] ].

*Conclusion.*—Unlike equilibrium systems, self-driven active particles can self-organize into a liquid and a coexisting gas phase at different temperatures. This result exemplifies a route to use self-driven particles to create a self-sustained temperature gradient, which might serve, in principle, as a novel paradigm to create isolating layers

at the microscale, e.g., to keep bodies at different temperatures.

On a more fundamental level, our results show that motility-induced phase separation, one of the best explored phenomena in active matter research, is fundamentally different from a liquid-gas phase separation—an insight which has been curtained by the focus on overdamped particles so far. As a consequence, the phenomenology of motility-induced phase separation is even richer than anticipated previously—it can, in particular, lead to phenomena at the macroscale that are fundamentally beyond equilibrium physics.

For future studies, it would also be interesting to study the effect of inertia on anisotropic active particles [48–51] where translational and rotational motions are coupled. Specifically for such particles, Ref. [52] has recently observed (but hardly analyzed) the occurrence of different kinetic energies in coexisting phases, suggesting that the present findings survive for particles of nonspherical shape. An interesting challenge would also be to derive a microscopic theory for motility-induced phase separation in underdamped particles to predict the joint temperature and density profiles across the interface between the two coexisting states [53]. Such an approach needs to be designed for nonisothermal situations as considered recently in Enskog kinetic theories [54,55] or in dynamical density functional theory [56,57].

We thank Christian Scholz and Alexei Ivlev for fruitful discussions. This work is supported by the German Research Foundation (Grant No. LO 418/23-1).

*mandal@hhu.de
†liebchen@fkp.tu-darmstadt.de
‡hlowen@hhu.de

[1] P. Romanczuk, M. Bär, W. Ebeling, B. Lindner, and L. Schimansky-Geier, Active Brownian particles, Eur. Phys. J. Spec. Top. **202**, 1 (2012).
[2] M. E. Cates and J. Tailleur, Motility-induced phase separation, Annu. Rev. Condens. Matter Phys. **6**, 219 (2015).
[3] R. Ni, M. A. C. Stuart, and M. Dijkstra, Pushing the glass transition towards random close packing using self-propelled hard spheres, Nat. Commun. **4**, 2704 (2013).
[4] C. Kurzthaler, C. Devailly, J. Arlt, T. Franosch, W. C. K. Poon, V. A. Martinez, and A. T. Brown, Probing the Spatiotemporal Dynamics of Catalytic Janus Particles with Single-Particle Tracking and Differential Dynamic Microscopy, Phys. Rev. Lett. **121**, 078001 (2018).
[5] R. G. Winkler, A. Wysocki, and G. Gompper, Virial pressure in systems of spherical active Brownian particles, Soft Matter **11**, 6680 (2015).
[6] J. Tailleur and M. E. Cates, Statistical Mechanics of Interacting Run-and-Tumble Bacteria, Phys. Rev. Lett. **100**, 218103 (2008).
[7] Y. Fily and M. C. Marchetti, Athermal Phase Separation of Self-Propelled Particles with No Alignment, Phys. Rev. Lett. **108**, 235702 (2012).
[8] A. Patch, D. M. Sussman, D. Yllanes, and M. C. Marchetti, Curvature-dependent tension and tangential flows at the interface of motility-induced phases, Soft Matter **14**, 7435 (2018).
[9] I. Buttinoni, J. Bialké, F. Kümmel, H. Löwen, C. Bechinger, and T. Speck, Dynamical Clustering and Phase Separation in Suspensions of Self-Propelled Colloidal Particles, Phys. Rev. Lett. **110**, 238301 (2013).
[10] J. Stenhammar, A. Tiribocchi, R. J. Allen, D. Marenduzzo, and M. E. Cates, Continuum Theory of Phase Separation Kinetics for Active Brownian Particles, Phys. Rev. Lett. **111**, 145702 (2013).
[11] J. Stenhammar, D. Marenduzzo, R. J. Allen, and M. E. Cates, Phase behaviour of active Brownian particles: The role of dimensionality, Soft Matter **10**, 1489 (2014).
[12] G. S. Redner, M. F. Hagan, and A. Baskaran, Structure and Dynamics of a Phase-Separating Active Colloidal Fluid, Phys. Rev. Lett. **110**, 055701 (2013).
[13] P. Digregorio, D. Levis, A. Suma, L. F. Cugliandolo, G. Gonnella, and I. Pagonabarraga, Full Phase Diagram of Active Brownian Disks: From Melting to Motility-Induced Phase Separation, Phys. Rev. Lett. **121**, 098003 (2018).
[14] Z. Mokhtari, T. Aspelmeier, and A. Zippelius, Collective rotations of active particles interacting with obstacles, Europhys. Lett. **120**, 14001 (2017).
[15] A. P. Solon, J. Stenhammar, M. E. Cates, Y. Kafri, and J. Tailleur, Generalized thermodynamics of motility-induced phase separation: Phase equilibria, laplace pressure, and change of ensembles, New J. Phys. **20**, 075001 (2018).
[16] D. Levis, J. Codina, and I. Pagonabarraga, Active Brownian equation of state: Metastability and phase coexistence, Soft Matter **13**, 8113 (2017).
[17] J. T. Siebert, F. Dittrich, F. Schmid, K. Binder, T. Speck, and P. Virnau, Critical behavior of active Brownian particles, Phys. Rev. E **98**, 030601(R) (2018).
[18] J. Elgeti, R. G. Winkler, and G. Gompper, Physics of microswimmers—single particle motion and collective behavior: A review, Rep. Prog. Phys. **78**, 056601 (2015).
[19] C. Bechinger, R. Di Leonardo, H. Löwen, C. Reichhardt, G. Volpe, and G. Volpe, Active particles in complex and crowded environments, Rev. Mod. Phys. **88**, 045006 (2016).
[20] H.-W. Huang, F. E. Uslu, P. Katsamba, E. Lauga, M. Sakar, and B. Nelson, Adaptive locomotion of artificial microswimmers, Sci. Adv. **5**, eaau1532 (2019).
[21] A. Aubret, S. Ramananarivo, and J. Palacci, Eppur si muove, and yet it moves: Patchy (phoretic) swimmers, Curr. Opin. Colloid Interface Sci. **30**, 81 (2017).
[22] A. Aubret and J. Palacci, Diffusiophoretic design of self-spinning microgears from colloidal microswimmers, Soft Matter **14**, 9577 (2018).
[23] C. Maggi, M. Paoluzzi, L. Angelani, and R. Di Leonardo, Memory-less response and violation of the fluctuation-dissipation theorem in colloids suspended in an active bath, Sci. Rep. **7**, 17588 (2017).
[24] H. Mukundarajan, T. C. Bardon, D. H. Kim, and M. Prakash, Surface tension dominates insect flight on fluid interfaces, J. Exp. Biol. **219**, 752 (2016).

[25] J. Rabault, R. A. Fauli, and A. Carlson, Curving to Fly: Synthetic Adaptation Unveils Optimal Flight Performance of Whirling Fruits, Phys. Rev. Lett. **122**, 024501 (2019).
[26] C. Scholz, S. Jahanshahi, A. Ldov, and H. Löwen, Inertial delay of self-propelled particles, Nat. Commun. **9**, 5156 (2018).
[27] G. E. Morfill and A. V. Ivlev, Complex plasmas: An interdisciplinary research field, Rev. Mod. Phys. **81**, 1353 (2009).
[28] A. Suma, G. Gonnella, D. Marenduzzo, and E. Orlandini, Motility-induced phase separation in an active dumbbell fluid, Europhys. Lett. **108**, 56004 (2014).
[29] L. F. Cugliandolo, The effective temperature, J. Phys. A **44**, 483001 (2011).
[30] C. Nardini, E. Fodor, E. Tjhung, F. van Wijland, J. Tailleur, and M. E. Cates, Entropy Production in Field Theories Without Time-Reversal Symmetry: Quantifying the Non-Equilibrium Character of Active Matter, Phys. Rev. X **7**, 021007 (2017).
[31] D. Levis and L. Berthier, From single-particle to collective effective temperatures in an active fluid of self-propelled particles, Europhys. Lett. **111**, 60006 (2015).
[32] Z. Preisler and M. Dijkstra, Configurational entropy and effective temperature in systems of active Brownian particles, Soft Matter **12**, 6043 (2016).
[33] See Supplemental Material at http://link.aps.org/supplemental/10.1103/PhysRevLett.123.228001, which includes Refs. [34–38], for details on the underdamped simulations, the bouncing ball picture, the virial temperature, and the slow coarsening, Fig. S4, movies S1 and S2, and a description of the movies.
[34] J. D. Weeks, D. Chandler, and H. C. Andersen, Role of repulsive forces in determining the equilibrium structure of simple liquids, J. Chem. Phys. **54**, 5237 (1971).
[35] Q.-L. Lei, M. P. Ciamarra, and R. Ni, Nonequilibrium strongly hyperuniform fluids of circle active particles with large local density fluctuations, Sci. Adv. **5**, eaau7423 (2019).
[36] C. Rycroft, Voro++: A three-dimensional voronoi cell library in C++, Chaos **19**, 041111 (2009).
[37] P. M. Chaikin and T. C. Lubensky, *Principles of Condensed Matter Physics* (Cambridge University Press, Cambridge, England, 2000).
[38] S. K. Das, S. Roy, and J. Midya, Coarsening in fluid phase transitions, C. R. Phys. **16**, 303 (2015).
[39] Y. Komatsu and H. Tanaka, Roles of Energy Dissipation in a Liquid-Solid Transition of Out-of-Equilibrium Systems, Phys. Rev. X **5**, 031025 (2015).
[40] K. Roeller, J. P. D. Clewett, R. M. Bowley, S. Herminghaus, and M. R. Swift, Liquid-Gas Phase Separation in Confined Vibrated Dry Granular Matter, Phys. Rev. Lett. **107**, 048002 (2011).
[41] T. Schindler and S. C. Kapfer, Nonequilibrium steady states, coexistence, and criticality in driven quasi-two-dimensional granular matter, Phys. Rev. E **99**, 022902 (2019).
[42] P. Krinninger, M. Schmidt, and J. M. Brader, Nonequilibrium Phase Behavior from Minimization of Free Power Dissipation, Phys. Rev. Lett. **117**, 208003 (2016).
[43] A. P. Solon, J. Stenhammar, M. E. Cates, Y. Kafri, and J. Tailleur, Generalized thermodynamics of phase equilibria in scalar active matter, Phys. Rev. E **97**, 020602(R) (2018).
[44] T. Speck, J. Bialké, A. M. Menzel, and H. Löwen, Effective Cahn-Hilliard Equation for the Phase Separation of Active Brownian Particles, Phys. Rev. Lett. **112**, 218304 (2014).
[45] A. Wysocki, R. G. Winkler, and G. Gompper, Cooperative motion of active Brownian spheres in three-dimensional dense suspensions, Europhys. Lett. **105**, 48004 (2014).
[46] S. Plimpton, Fast parallel algorithms for short-range molecular dynamics, J. Comput. Phys. **117**, 1 (1995).
[47] C. Scholz and T. Pöschel, Velocity Distribution of a Homogeneously Driven Two-Dimensional Granular Gas, Phys. Rev. Lett. **118**, 198003 (2017).
[48] N. H. P. Nguyen, D. Klotsa, M. Engel, and S. C. Glotzer, Emergent Collective Phenomena in a Mixture of Hard Shapes through Active Rotation, Phys. Rev. Lett. **112**, 075701 (2014).
[49] S. Farhadi, S. Machaca, J. Aird, B. O. T. Maldonado, S. Davis, P. E. Arratia, and D. J. Durian, Dynamics and thermodynamics of air-driven active spinners, Soft Matter **14**, 5588 (2018).
[50] G. Kokot, S. Das, R. G. Winkler, G. Gompper, I. S. Aranson, and A. Snezhko, Active turbulence in a gas of self-assembled spinners, Proc. Natl. Acad. Sci. U.S.A. **114**, 12870 (2017).
[51] A. Aubret, M. Youssef, S. Sacanna, and J. Palacci, Targeted assembly and synchronization of self-spinning microgears, Nat. Phys. **14**, 1114 (2018).
[52] I. Petrelli, P. Digregorio, L. F. Cugliandolo, G. Gonnella, and A. Suma, Active dumbbells: Dynamics and morphology in the coexisting region, Eur. Phys. J. E **41**, 128 (2018).
[53] K. Miyazaki, Y. Nakayama, and H. Matsuyama, Entropy anomaly and linear irreversible thermodynamics, Phys. Rev. E **98**, 022101 (2018).
[54] J. J. Brey, V. Buzón, P. Maynar, and M. I. García de Soria, Hydrodynamics for a model of a confined quasi-two-dimensional granular gas, Phys. Rev. E **91**, 052201 (2015).
[55] V. Garzó, R. Brito, and R. Soto, Enskog kinetic theory for a model of a confined quasi-two-dimensional granular fluid, Phys. Rev. E **98**, 052904 (2018).
[56] R. Wittkowski, H. Löwen, and H. R. Brand, Extended dynamical density functional theory for colloidal mixtures with temperature gradients, J. Chem. Phys. **137**, 224904 (2012).
[57] J. G. Anero, P. Español, and P. Tarazona, Functional thermodynamics: A generalization of dynamic density functional theory to non-isothermal situations, J. Chem. Phys. **139**, 034106 (2013).